Asian Journal of Chemistry; Vol. 34, No. 1 (2022), 239-244

ASIAN JOURNAL OF CHEMISTRY

https://doi.org/10.14233/ajchem.2022.23495

Thermal Decomposition of Copper Acetate at Various Temperature and Time to form Copper Oxide/Copper Nanoparticles

S.B. SIBOKOZA[1,*], M.J. MOLOTO[2], F. MTUNZI[1] and N. MOLOTO[3]

[1]Department of Chemistry, Vaal University of Technology, Private Bag X 021, Vanderbijlpark, 1900, South Africa
[2]Institute for Nanotechnology and Water Sustainability, University of South Africa, 28 Pioneer road, Florida Park, Roodeport, 1709, South Africa
[3]School of Chemistry, University of the Witwatersrand, Private Bag 3, Wits, 2050, South Africa

*Corresponding author: Tel: +27 169509816; E-mail: simons@vut.ac.za

Received: 22 August 2021; *Accepted*: 1 November 2021; *Published online*: 16 December 2021; AJC-20642

In the present study, the copper oxide and copper nanoparticles were prepared by thermal decomposition of solid phase copper acetate at various time (1-3 h) and temperature (200-500 ºC). The method is simple, less expensive, avoid toxic solvent as well as avoid use of passivating agents. The FT-IR spectrum of the copper acetate monohydrate (calcined) shows the major changes in absorption peaks associated with methyl, carbon-oxygen double bond, carbon-oxygen single bond and copper-oxygen bond functional groups. Thermogravimetry analysis shows that the copper acetate monohydrate decomposes at about 250 ºC to form copper. The TEM images show a combination of shapes, which includes icosahedrons, truncated cubes and nano-whiskers made from sphere with diameter of 7.43-0.83 nm.

Keywords: Copper acetate, Copper oxide, Copper, Temperature, Time, Nanoparticles.

INTRODUCTION

Copper oxide exists in three stoichiometric which include cuprous oxide (Cu_2O, cuprite), cupric oxide (CuO, tenorite) and Cu_4O_3 (paramelaconite) with their crystalline forms [1]. All the copper oxides are p-type semiconductor with a narrow band gap in the range between 1.2 to 2.5 eV depending on their stoichiometry [2,3]. Copper oxide shows unique physical, electronic and photonic properties [4], which have led to its application in sensors, catalysis, batteries, high-temperature superconductors, solar energy and magnetic storage media [5]. Copper base compounds are known for their biocidal properties, which include antimicrobial, antibiotic and antifungal agent [6]. Copper oxide shows better biocidal properties than most organic antimicrobial agents, because of it's stability, strength and tends to possess long shelf life [7,8]. Copper oxide nanoparticles have been prepared using many methods, which includes sol-gel [9], thermal oxidation of copper substrates [10], solvothermal [11], solid state reaction [12], electrochemical [13], hydrothermal [14], precipitation methods [15] and thermal decomposition of single precursor [16].

The single-source precursor involves a compound (salt or complex) with both metal (copper) and chalcogenide containing ligand (oxygen) [17]. The single-source precursor allows easy control of reaction conditions and leads to nanoparticles with well-defined size and shape [18]. In general, single-source precursor involves the synthesis of complexes from metal salts (metal source) and ligand (chalcogenide source) [19]. The complex can be thermalized to form metal chalcogenide nanoparticles in the presence of a passivating agent to control the growth of nanoparticles [20]. Metal acetate salts can also be used as a single-source precursor for the preparation of metal oxide nanoparticles [21,22]. Copper acetate is easy to handle, low cost and with both metal (copper) and chalcogenide (oxygen) in one source. The furnace makes it possible to thermally decompose the compound without the use of a passivating agent. This article reports a simple, convenient and passivating free method to prepare copper oxide nanoparticles. The method involves thermal decomposition of copper acetate monohydrate precursor under solid state conditions. Thermal decomposition temperature and reaction time varied to study their effect on the growth of nanoparticles.

EXPERIMENTAL

Copper acetate monohydrate (99.0%) was purchased from Merck, USA, while toluene (99.5%) was purchased at Sigma-Aldrich. All the chemicals were of analytical grade and used without any further purification.

Synthesis of copper oxide nanoparticles: Copper acetate monohydrate (0.5 g) was placed inside a small, square piece of aluminium foil. The foil was placed in the glass tube and put into the furnace purged with nitrogen. The sample was calcined for 1 h at 200 ºC. After 1 h, the sample was cool to room temperature while inside the furnace. Then, the sample was ready to be characterized. The method was repeated at 300, 400 and 500 ºC for 1 h. The same procedure was repeated at a various time interval (180, 150, 120, 90, 60) min at 300 ºC.

Characterization: Infrared spectra were recorded on the Thermo-Scientific Nicolet iS50FT-IR spectrometer. The spectra were collected over the range of 4000 to 400 cm^{-1}. Thermogravimetric analysis was performed using Perkin-Elmer Pyris 6 TGA under an inert atmosphere of dry nitrogen. The compounds were heated from 30 to 800 ºC at a heating rate of 10 ºC min^{-1}. Powder X-ray diffraction patterns were recorded using a Shimadzu XRD 700 X-ray diffract meter diffractometer with Cu*K*α radiation (λ = 1.54 Å) at 40 kV and 40 mA. The samples were scanned within a 2θ range of 10-80º in a step size of 0.05% with a count rate of 9 s. Transmission electron microscope (TEM) analysis was performed using HITACHI JEOL 100S operated at 80 kV. All the samples were deposited on carbon-coated copper grids and allowed to dry.

RESULTS AND DISCUSSION

The FTIR spectra of copper acetate monohydrate (Fig. 1) and the FT-IR peaks are assigned according to their functional groups in Table-1. The FTIR show three absorption peaks of interest: the first peaks at 3465-3268 cm^{-1}, due to a hydroxyl group of water and acetic acid [23]. Second peaks at 2993 and 2945 cm^{-1} (weak), which are attributed to the methyl group. Third absorption peaks at 1594 and 1417 cm^{-1}, which can be associated to symmetric and antisymmetric carboxylate stretching mode [24,25].

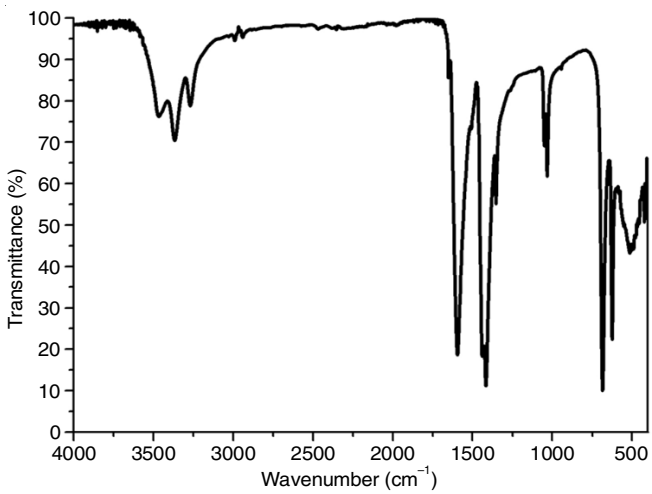

Fig. 1. FT-IR spectrum of copper acetate monohydrate

TABLE-1
FTIR SPECTRA OF COPPER ACETATE MONOHYDRATE

Wavenumber (cm^{-1})	Assignment
3465	O–H stretching in crystal water
3365	O–H stretching in acetic acid
3268	O–H stretching in crystal water
2993	C–H stretching in methyl
2945	C–H stretching in methyl
1651	HOH bending
1354	C–H bending in methyl
1049	C–CH_3 framework vibration
1032	C–CH_3 framework vibration
1594	C=O stretching
1417	C=O stretching, C–H bending in methyl
685	Acetate anion scissoring
625	Acetate anion twisting

Fig. 2 shows the TGA (black) and DTG (red) curves of copper acetate monohydrate. Copper acetate monohydrate decomposes into two steps (**Scheme-I**) [26]. The first decomposition occurs between 111 and 159 ºC, which is associated with dehydration [23]. The dehydration led to a mass loss of 8.28% and comparable with water molecule theoretical (9.02%) [26]. The second decomposition occurs between 208 and 317 ºC and was due to acetate moiety [27]. The decomposition of acetate resulted in a mass loss of 59.29%, which is in good agreement with theoretical value (59.16%). A copper residue with a mass of 32.43% was comparable with theoretical (31.83%). The DTG (red) show three endothermic peaks at 143, 269 and 288 ºC. The DTG peaks at 143 and 288 ºC were consistent with dehydration and decomposition of acetate moiety, respectively [25]. The DTG peak at 269 ºC could be associated with copper oxide intermediates which further composed into copper.

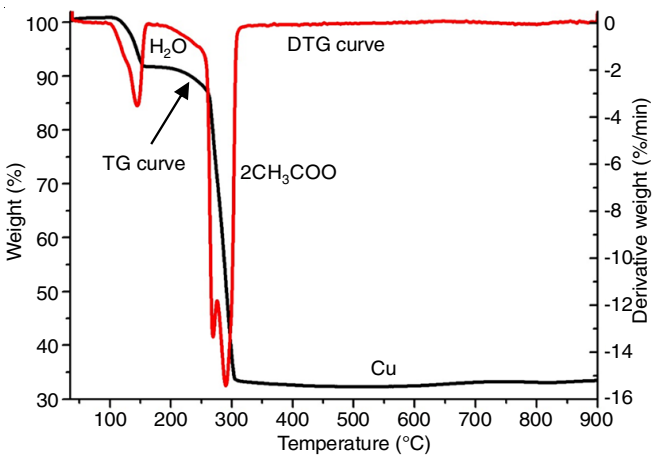

Fig. 2. Thermogravimetric analysis curve (black) and derivative (red) for copper acetate monohydrate

Effect of time: Fig. 3 shows the FT-IR spectra of $Cu(OAc)_2 \cdot H_2O$ and $Cu(OAc)_2 \cdot H_2O$ calcined at 300 ºC and a various time interval of reaction (1-3 h). The spectra show that significant changes occur in functional groups associated with hydroxyl, methyl, carbonyl and copper-oxygen. The $Cu(OAc)_2 \cdot H_2O$ (uncalcined) showed O-H group (water) peaks at 3465-3268 cm^{-1}, while these peaks are not present in calcined $Cu(OAc)_2 \cdot H_2O$.

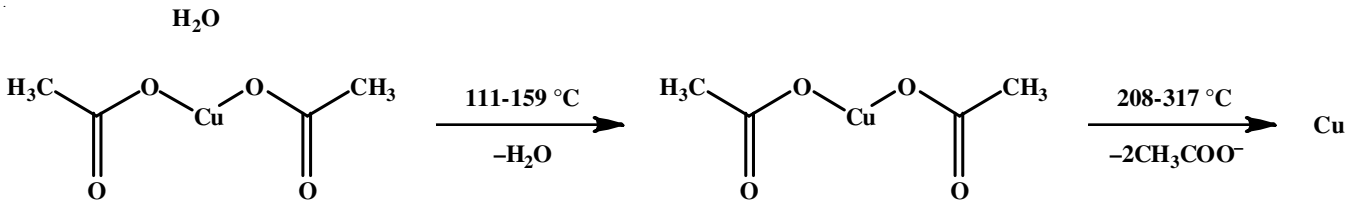

Scheme-I: Reaction pathway involved in thermal decomposition of $Cu(OAc)_2·H_2O$ in the presence of nitrogen

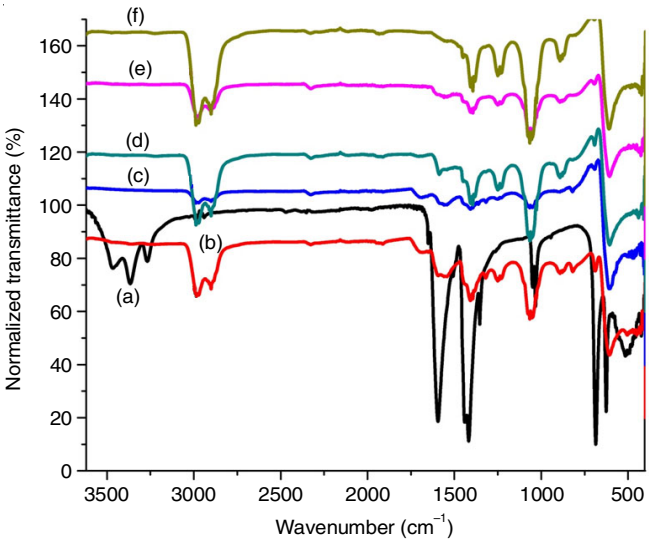

Fig. 3. FTIR spectra of $Cu(OAc)_2·H_2O$ (a) and $Cu(OAc)_2·H_2O$ calcined at 300 ºC by varying time (min): 60 (b), 90 (c), 120 (d), 150 (e), 180 (f)

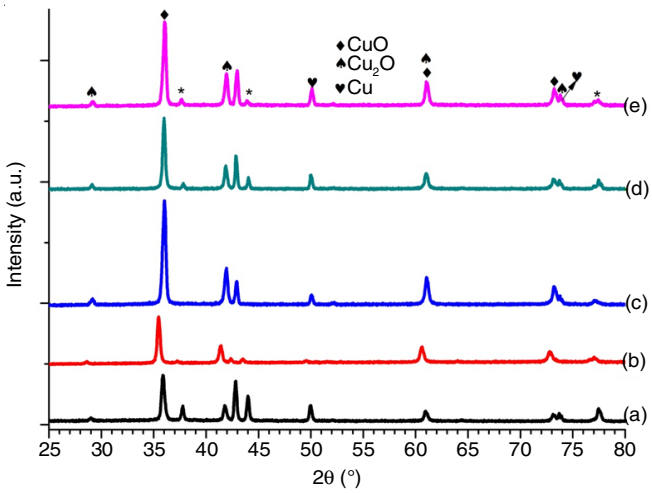

Fig. 4. XRD spectra of $Cu(OAc)_2·H_2O$ calcined at 300 ºC by varying time (min): 60 (a), 90 (b), 120 (c), 150 (d), 180 (e)

The disappearance of hydroxyl group peaks in calcined samples confirms that water molecule had been driven off from calcined copper acetate. The second peaks appear at 2993 and 2945 cm^{-1} are due to the methyl group. These peaks were very weak for $Cu(OAc)_2·H_2O$ (uncalcined), since their intensity were supressed by more instense functional groups of O-H and C=O. The methyl group peaks were more vissible for all calcined $Cu(OAc)_2·H_2O$ sample, because the function (O-H and C=O), which were hindrance to there have been decreased or are no longer present. The third peaks at 1651 and 1417 cm^{-1} is attributed to carbon-oxygen double bond. The peak at 1651 cm^{-1} was intensive for uncalcined $Cu(OAc)_2·H_2O$, while decreased and complete disappeared for calcined $Cu(OAc)_2·H_2O$. The fourth peak in 1240 cm^{-1} was due to carbon-oxygen single bond and present only in calcined $Cu(OAc)_2·H_2O$. This confirms that the carbon-oxygen double bond was converted to a single bond.

Fig. 4 shows the XRD pattern of $Cu(OAc)_2·H_2O$ calcined at 300 ºC by varying reaction time (1-3 h). The spectra show a mixture of three copper which includes cuprous oxide (Cu_2O, cuprite), cupric oxide (CuO, tenorite) and copper. All the samples show the same phases thought the reaction time, similar results at this temperature were reported [28]. The cuprous oxide peaks are consistent with cubic phase Cu_2O (JCPDS card number: 75-1531). However, the cupric oxide peaks can be indexed to a monoclinic structure of CuO (JCPDS card number: 80-1916). Furthermore, the XRD pattern for Cu can be indexed to the face-centered cubic Cu (JCPDS card number 85-1326) [16]. The peaks signified by the asterisk are due to sample holder because of smaller yield.

Fig. 5 shows the TEM images of $Cu(OAc)_2·H_2O$ calcined at 300 ºC by varying reaction time (1-3 h). The TEM shows bigger cluster with icosahedron shape made up of small copper oxide nanoparticles Fig. 5a. The small particles have a spherical shape with a diameter in size range of 7 to 2 nm. However, nanoparticles prepared from 90-150 min showed a mixture of an icosahedron and truncated cube with bigger particle sizes. These particles are agglomerated and made up of small particles (Fig. 5b-d). Furthermore, particles prepared at 180 min are spherical with a diameter in the range of 7 to 3 nm.

Effect of temperature: Fig. 6 shows the FI-IR spectra of $Cu(OAc)_2·H_2O$ (uncalcined) and $Cu(OAc)_2·H_2O$ calcined for 1 h, at various temperature of reaction (200-500 ºC). The spectra show similar results as for $Cu(OAc)_2·H_2O$ calcined at 300 ºC and various time as outlined in Fig. 3. The $Cu(OAc)_2·H_2O$ uncalcined and $Cu(OAc)_2·H_2O$ calcined at 200 ºC show spectra at the same peaks, except that the peak intensity has decreased for calcined samples. This shows that only water that is evaporating at this temperature range and some hydroxyl group peaks are still present at low intensity. However, $Cu(OAc)_2·H_2O$ calcined at the range of 300-500 ºC show major changes in the spectra compared to uncalcined $Cu(OAc)_2·H_2O$. Firstly peaks at 3465-3268 cm^{-1} (uncalcined) due to the hydroxyl group of crystal water are not present for $Cu(OAc)_2·H_2O$ calcined at 300-500 ºC. The second peaks at 2993 and 2945 cm^{-1} due to methyl group are sharp and intense for $Cu(OAc)_2·H_2O$ calcined at 300-500 ºC. These peaks are very weak for uncalcined $Cu(OAc)_2·H_2O$. The third peaks at 1651-1417 cm^{-1} are weak and disappearing as the temperature is increased. These carbonyl and hydroxyl group are stronger on the uncalcined $Cu(OAc)_2·H_2O$ sample.

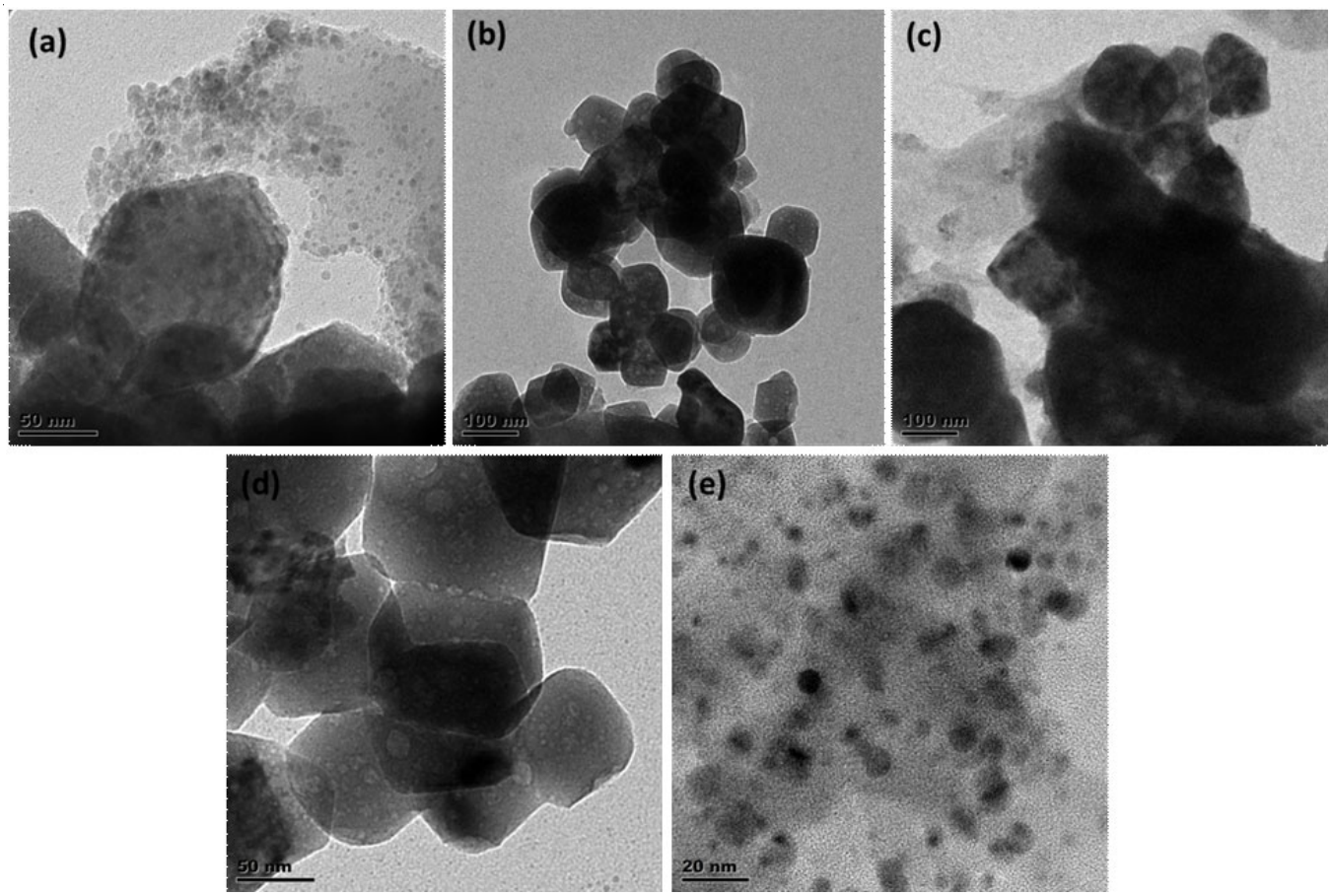

Fig. 5. TEM images of $Cu(OAc)_2{\cdot}H_2O$ calcined at 300 ºC by varying time (min): 60 (a), 90 (b), 120 (c), 150 (d), 180 (e)

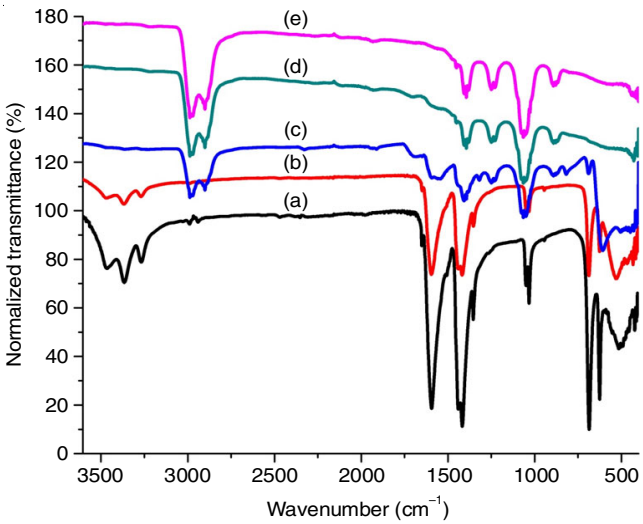

Fig. 6. FTIR spectra of $Cu(OAc)_2{\cdot}H_2O$ (a) and $Cu(OAc)_2{\cdot}H_2O$ calcined for 60 min at various temperatures (ºC): 200 (b), 300 (c), 400 (d), 500 (e)

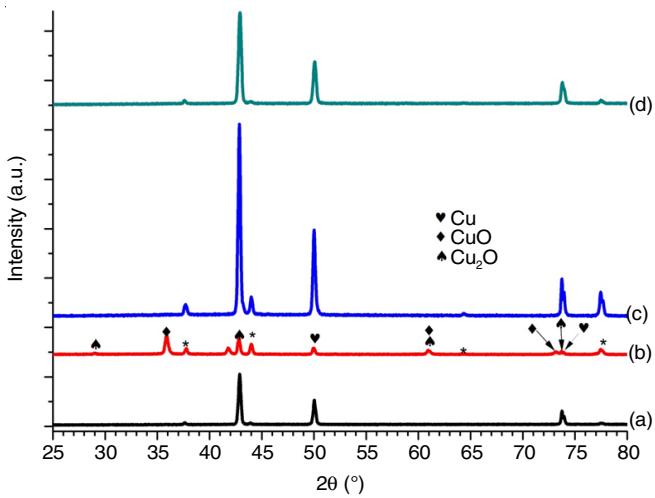

Fig. 7. XRD spectra of $Cu(OAc)_2{\cdot}H_2O$ (a) and $Cu(OAc)_2{\cdot}H_2O$ calcined for 60 min at various temperatures (°C): 200 (a), 300 (b), 400 (c), 500 (d)

The disappearance of carbonyl group confirms that oxygen is used to fully bond with copper or decomposing as temperature is increased.

Fig. 7 shows the XRD pattern of $Cu(OAc)_2{\cdot}H_2O$ calcined for 1 h by varying temperature (200, 300, 400 and 500 ºC). The spectra show a mixture of three copper, which includes cuprous oxide (Cu_2O, cuprite), cupric oxide (CuO, tenorite) and copper. The spectra for $Cu(OAc)_2{\cdot}H_2O$ calcined at 200, 400 and 500 ºC show a mixture of cuprous oxide and copper. However, the spectra for $Cu(OAc)_2{\cdot}H_2O$ calcined show a combination of three-phase which include cuprous oxide, cupric oxide and copper. The cuprous oxide peaks are consistent with cubic phase Cu_2O (JCPDS card number: 75-1531). However, the cupric oxide peaks can be indexed to a monoclinic structure of CuO (JCPDS card number: 80-1916). Furthermore, the

XRD pattern for Cu can be indexed to the face-centered cubic Cu(JCPDS card number 85-1326) [16]. The peaks signified by an asterisk are due to sample holder because of smaller yield. The sample holder peaks appear due to lower sample yield.

Fig. 8 shows the TEM images of $Cu(OAc)_2·H_2O$ calcined for 1 h and by varying temperature (200-500 ºC). The image for $Cu(OAc)_2·H_2O$ calcined at 200 ºC show agglomerated nanowhiskers. As the temperature was increased to 300 ºC, the clusters with icosahedron shape build up by spherical nanoparticles of 7-2 nm diameter. For nanoparticles prepared at 400 ºC show a well dispersed spherically shaped nanoparticles with a diameter in the range of 6-3 nm. However, for $Cu(OAc)_2·H_2O$ calcined at 500 ºC show TEM image with well dispersed spherically shaped nanoparticles with a diameter of 1-3 nm.

Conclusion

Copper oxide nanoparticles were prepared by the thermal decomposition of solid copper acetate monohydrate. The FT-IR spectra for calcined $Cu(OAc)_2·H_2O$ showed changes in absorption peaks attributed to methyl, carbon-oxygen double bond, carbon oxygen single bond, copper-oxygen group as compared to $Cu(OAc)_2·H_2O$ (uncalcined). Thermogravimetric analysis showed that $Cu(OAc)_2·H_2O$ decomposes above 250 ºC to form copper oxide intermediate which further decomposes into copper. The XRD showed that $Cu(OAc)_2·H_2O$ decomposed to

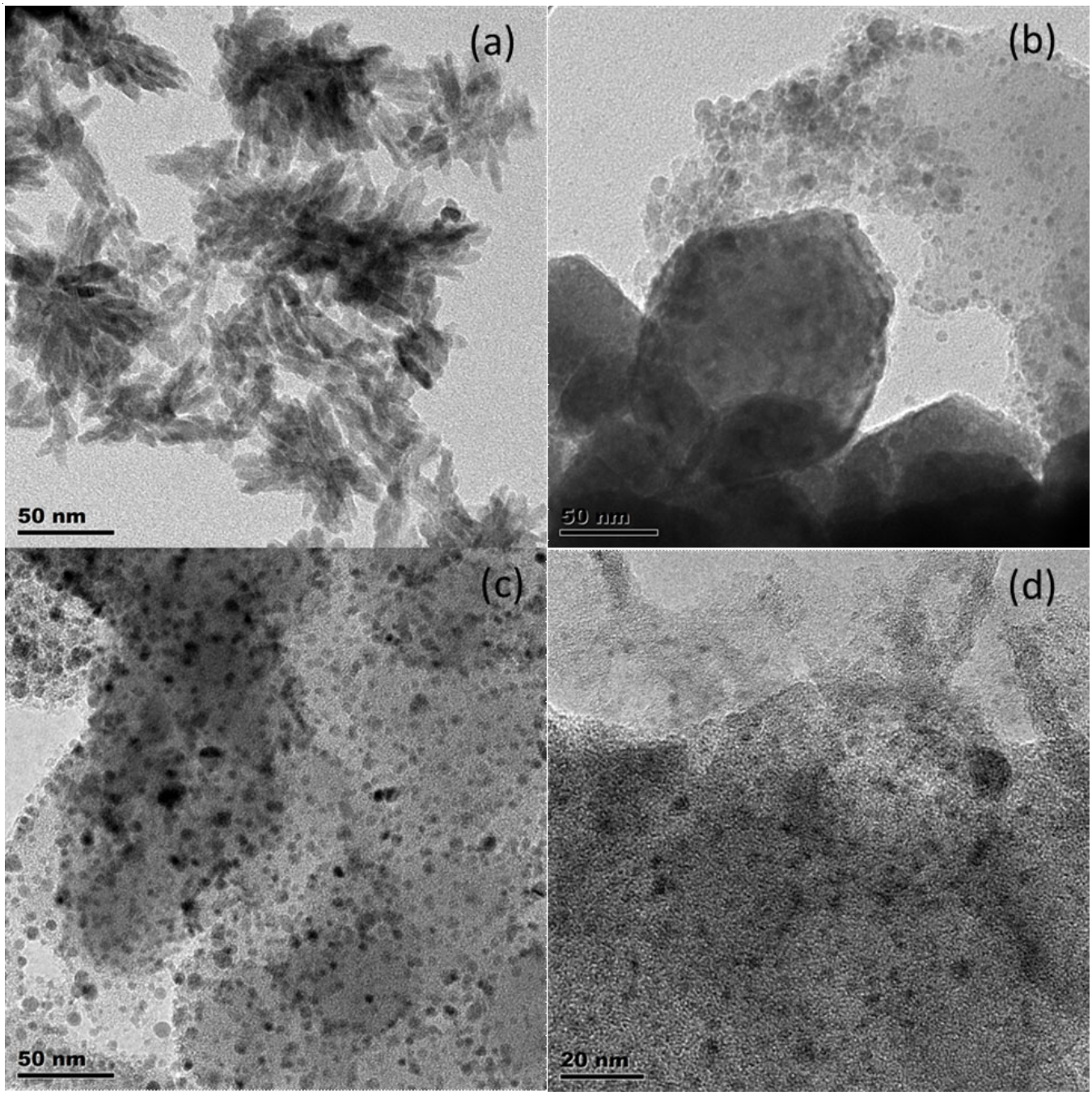

Fig. 8. TEM images of $CuAc_2·H_2O$ calcined for 60 min at various temperatures (°C): 200 (a), 300 (b), 400 (c), 500 (d)

form three copper nanoparticles: cuprite, tenorite and copper. The TEM images showed many shapes which include icosahedrons, truncated tubes, nanowhiskers and small spheres. The images showed that nanospheres were the build block for icosahedron truncated tubes and nanowhiskers. The solid solid-state reaction conditions such as short time and low temperatures favour agglomerated copper oxide nanoparticles. However, longer time and high temperatures favour spheres with diameter in the range of 2-7 and 1-6 nm.

ACKNOWLEDGEMENTS

The authors acknowledge national research foundation, South Africa (NRF) and Vaal University of Technology.

CONFLICT OF INTEREST

The authors declare that there is no conflict of interests regarding the publication of this article.

REFERENCES

1. C.-H. Wang, H.-L. Tsai and W.-S. Hwang, *Materials*, **9**, 1 (2016); https://doi.org/10.3390/ma10010001
2. C.-Y. Chiang, Y. Shin and S. Ehrman, *Energy Procedia*, **61**, 1799 (2014); https://doi.org/10.1016/j.egypro.2014.12.216
3. A. Shui, W. Zhu, L. Xu, D. Qin and Y. Wang, *Ceram. Int.*, **39**, 8715 (2013); https://doi.org/10.1016/j.ceramint.2013.04.055
4. T. Jiang, Y. Wang, D. Meng, X. Wu, J. Wang and J. Chen, *Appl. Surf. Sci.*, **311**, 602 (2014); https://doi.org/10.1016/j.apsusc.2014.05.116
5. R. Sivaraj, P.K.S.M. Rahman, P. Rajiv, S. Narendhran and R. Venckatesh, *Biomol. Spectrosc.*, **129**, 255 (2014); https://doi.org/10.1016/j.saa.2014.03.027
6. G. Borkow and J. Gabbay, *Curr. Chem. Biol.*, **3**, 272 (2009); https://doi.org/10.2174/187231309789054887
7. G. Ren, D. Hu, E.W.C. Cheng, M.A. Vargas-Reus, P. Reip and R.P. Allaker, *Int. J. Antimicrob. Agents*, **33**, 587 (2009); https://doi.org/10.1016/j.ijantimicag.2008.12.004
8. M. Raffi, S. Mehrwan, T.M. Bhatti, J.I. Akhter, A. Hameed, W. Yawar, M.M. ul Hasan, *Ann. Microbiol.*, **60**, 75 (2010); https://doi.org/10.1007/s13213-010-0015-6
9. J. Jang, S. Chung, H. Kang and V. Subramanian, *Thin Solid Films*, **600**, 157 (2016); https://doi.org/10.1016/j.tsf.2016.01.036
10. J.T. Chen, F. Zhang, J. Wang, G.A. Zhang, B.B. Miao, X.Y. Fan, D. Yan and P.X. Yan, *J. Alloys Compd.*, **454**, 268 (2008); https://doi.org/10.1016/j.jallcom.2006.12.032
11. L. Zhang, W. Lu, J. Ni, Y. Lu and X. Shang, *Wuli Huaxue Xuebao*, **24**, 2257 (2008).
12. W. Wang, Y. Zhan, X. Wang, Y. Liu, C. Zheng and G. Wang, *Mater. Res. Bull.*, **37**, 1093 (2002); https://doi.org/10.1016/S0025-5408(02)00745-6
13. N. Liu, D. Wu, H. Wu, C. Liu and F. Luo, *Mater. Chem. Phys.*, **107**, 511 (2008); https://doi.org/10.1016/j.matchemphys.2007.08.026
14. W. Jia, E. Reitz, P. Shimpi, E.G. Rodriguez, P. Gao and Y. Lei, *Mater. Res. Bull. J.*, **44**, 1681 (2009); https://doi.org/10.1016/j.materresbull.2009.04.003
15. R. Wu, Z. Ma, Z. Gu and Y. Yang, *J. Alloys Compd.*, **504**, 45 (2010); https://doi.org/10.1016/j.jallcom.2010.05.062
16. X. Liu, B. Geng, Q. Du, J. Ma and X. Liu, *Mater. Sci. Eng. A*, **448**, 7 (2007); https://doi.org/10.1016/j.msea.2006.08.104
17. T. Xaba, M.J. Moloto, M. Al-Shakban, M.A. Malik, P. O'Brien and N. Moloto, *Mater. Sci. Semicond. Process.*, **71**, 109 (2017); https://doi.org/10.1016/j.mssp.2017.07.015
18. K. Ramasamy, W. Maneerprakorn, M.A. Malik and P. O'Brien, *Phys. Eng. Sci.*, **368**, 4249 (2010); https://doi.org/10.1098/rsta.2010.0125
19. S.B. Sibokoza, M.J. Moloto, N. Moloto and P.N. Sibiya, *Chalcogenide Lett.*, **14**, 69 (2017).
20. T. Xaba, M.J. Moloto and N. Moloto, *Dig. J. Nanomater. Biostruct.*, **13**, 49 (2018).
21. S.D. Bakrania, G.K. Rathore and M.S. Wooldridge, *J. Therm. Anal. Calorim.*, **95**, 117 (2009); https://doi.org/10.1007/s10973-008-9173-1
22. R. Saravanan, S. Karthikeyan, V.K. Gupta, G. Sekaran, V. Narayanan and A. Stephen, *Mater. Sci. Eng. C*, **33**, 91 (2013); https://doi.org/10.1016/j.msec.2012.08.011
23. Z. Lin, D. Han and S. Li, *J. Therm. Anal. Calorim.*, **107**, 471 (2012); https://doi.org/10.1007/s10973-011-1454-4
24. Y. Kawaguchi, R. Arakawa, H. Kawasaki, *J. Coating Sci Technol.*, **3**, 56 56 (2016); https://doi.org/10.6000/2369-3355.2016.03.02.2
25. S.A.A. Mansour, *J. Therm. Anal.*, **46**, 263 (1996); https://doi.org/10.1007/BF01979966
26. J.V. Bellini, R. Machado, M.R. Morelli and R.H.G.A. Kiminami, *Mater. Res.*, **5**, 453 (2002); https://doi.org/10.1590/S1516-14392002000400010
27. A.Y. Obaid, A.O. Alyoubi, A.A. Samarkandy, S.A. Al-Thabaiti, S.S. Al-Juaid, A.A. El-Bellihi and E.-H.M. Deifallah, *J. Therm. Anal. Calorim.*, **61**, 985 (2000); https://doi.org/10.1023/A:1010179532267
28. Z. Lin, D. Han and S. Li, *J. Therm. Anal. Calorim.*, **107**, 471 (2012); https://doi.org/10.1007/s10973-011-1454-4